Received: 29 November 2022 | Revised: 30 May 2023 | Accepted: 2 June 2023

DOI: 10.1002/alz.13377

Alzheimer's & Dementia®
THE JOURNAL OF THE ALZHEIMER'S ASSOCIATION

RESEARCH ARTICLE

White matter hyperintensity longitudinal morphometric analysis in association with Alzheimer disease

Jeremy Fuller Strain[1] | **Chia-Ling Phuah**[1,2] | **Babatunde Adeyemo**[1] | **Kathleen Cheng**[1,3] | **Kyle B. Womack**[1] | **John McCarthy**[4] | **Manu Goyal**[5] | **Yasheng Chen**[1] | **Aristeidis Sotiras**[5,6] | **Hongyu An**[5] | **Chengjie Xiong**[7] | **Andrea Scharf**[8] | **Catherine Newsom-Stewart**[9] | **John Carl Morris**[1,10] | **Tammie Lee Smith Benzinger**[5,10] | **Jin-Moo Lee**[1,3,5] | **Beau M. Ances**[1,3,5,10] | **for the Alzheimer's Disease Neuroimaging Initiative**

[1]Department of Neurology, Washington University School of Medicine, St. Louis, Missouri, USA

[2]NeuroGenomics and Informatics Center, Washington University School of Medicine, St. Louis, Missouri, USA

[3]Department of Biomedical Engineering, Washington University in St. Louis, St. Louis, Missouri, USA

[4]Department of Mathematics, Washington University School of Medicine, St. Louis, Missouri, USA

[5]Department of Radiology, Washington University School of Medicine, St. Louis, Missouri, USA

[6]Institute for Informatics, Washington University School of Medicine, St. Louis, Missouri, USA

[7]Division of Biostatics, Washington University School of Medicine, St. Louis, Missouri, USA

[8]Department of Biological Sciences, Missouri University for Science and Technology, Rolla, Missouri, USA

[9]Department of Developmental Biology, Washington University School of Medicine, St. Louis, Missouri, USA

[10]Knight Alzheimer Disease Research Center, St. Louis, Missouri, USA

Correspondence
Jeremy Fuller Strain, Department of Neurology, Washington University School of Medicine, St. Louis, 1 Brookings Dr, Saint Louis, MO 63130, USA.
Email: strainj@wustl.edu

Funding information
National Institutes of Health, Grant/Award Number: U01 AG024904; National Institute on Aging; National Institute of Biomedical Imaging and Bioengineering, Grant/Award Numbers: R01 AG053550, K23 NS110927, R01AG052550, R01AG057680, R01AG067103, 19CDA34620004, P01 AG026276, R01 AG052550

Abstract

INTRODUCTION: Vascular damage in Alzheimer's disease (AD) has shown conflicting findings particularly when analyzing longitudinal data. We introduce white matter hyperintensity (WMH) longitudinal morphometric analysis (WLMA) that quantifies WMH expansion as the distance from lesion voxels to a region of interest boundary.

METHODS: WMH segmentation maps were derived from 270 longitudinal fluid-attenuated inversion recovery (FLAIR) ADNI images. WLMA was performed on five data-driven WMH patterns with distinct spatial distributions. Amyloid accumulation was evaluated with WMH expansion across the five WMH patterns.

RESULTS: The preclinical group had significantly greater expansion in the posterior ventricular WM compared to controls. Amyloid significantly associated with frontal WMH expansion primarily within AD individuals. WLMA outperformed WMH volume changes for classifying AD from controls primarily in periventricular and posterior WMH.

DISCUSSION: These data support the concept that localized WMH expansion continues to proliferate with amyloid accumulation throughout the entirety of the disease in distinct spatial locations.

KEYWORDS
AD, longitudinal, preclinical, WLMA, WMH

1 | BACKGROUND

The etiology of Alzheimer's disease (AD) has been described as the accumulation of beta-amyloid (Aβ), phosphorylated tau, and neurodegeneration leading to cognitive impairment.[1] Classically referred to as the ATN hypothesis, this evolving concept has expanded to infer vascular changes, but its role remains undefined in the pathophysiology of AD.[2] Pathological evidence suggests that a majority of individuals with AD have mixed pathology with concurrent vascular changes present. A commonly used method for measuring the severity of vascular changes is by quantifying regions of high intensity on fluid attenuated inversion recovery (FLAIR) images called white matter hyperintensities (WMH).[3] Vascular changes are inherently a risk factor for the development of not only AD but other neurodegenerative diseases. However, it remains unclear whether AD pathology includes vascular damage, or whether AD pathology and vascular damage are co-pathologies contributing to the AD process.[4]

In observational studies, increases in WMH are associated with both cumulative and longitudinal Aβ burden, even in healthy controls.[5] In contrast, WMH presence is less associated with cerebrospinal fluid t-tau or p-tau. In the ATN framework, amyloid accumulation occurs earlier in the disease suggesting that WMH changes might occur earlier in the AD process.[6] A known genetic risk factor for AD, the apolipoprotein (*APOE*) ε4 allele, is often associated with both elevated WMH presence and increased levels of Aβ supporting a related mechanism.[7] Prior works have shown that the presence of at least one *APOE* ε4 allele can promote cerebrovascular injury and is associated with earlier cognitive loss.[8,9] While the role of WMH in AD remains unclear, the aforementioned studies implicate WMH occurrence as potentially related to biomarkers and the severity of risk for AD.[10–12]

Growing evidence in neurodegenerative diseases has shown that WMH are heterogeneous and that the spatial location of WMH is more important than the cumulative WMH global burden for determining disease severity.[13,14] Global WMH summary metrics ignore specific regional effects and may undermine the sensitivity for detecting AD-specific WMH patterns. Prior strategies have focused on anatomical boundaries to evaluate regional specificity rather than spatially defined regions of interest (ROIs) based on WMH relationships with pathological markers.[12,15] A growing trend is to identify data-driven WMH spatial patterns in both healthy[16] and neurodegenerative populations.[17] Evaluating WMH patterns in AD has shown that certain patterns are distinct for vascular and amyloid risk factors.[17] WMH within the posterior white matter regions are uniquely associated with AD biomarkers implying the importance of analyzing location-specific WMH burden cross-sectionally. This demonstrates location-specific WMH that are associated with unique pathologies including AD and AD-related disorders. However, these findings are based on cross-sectional findings and it remains unclear whether these patterns persist for longitudinal analyses across AD severity.

Measurement of WMH volume has been the standard approach to quantifying lesion burden, but shape irregularity creates challenges for volume-based comparisons of location-specific WMH volume changes, particularly for longitudinal data. However, the evaluation of WMH shape changes that quantify changes of the lesion boundary across time are not restricted by these limitations. We propose a novel approach—white matter hyperintensity longitudinal morphometric analysis (WLMA)—for quantifying longitudinal WMH expansion to identify AD-specific longitudinal WMH change. Within each of the previously identified etiology-specific WM regions (juxtacortical, deep frontal, periventricular, parietal, and posterior),[17] we evaluated WMH change using WLMA compared to traditional volume for cognitively normal, preclinical, and symptomatic AD individuals. We further evaluated the contribution of *APOE* ε4 and amyloid on observed WMH change.

2 | METHODS

2.1 | Participants

Data utilized in this study were obtained from the Alzheimer's Disease Neuroimaging Initiative (ADNI) database (www.adni.loni.usc.edu), a private-public partnership established in 2003, led by the principal investigator Michael W. Weiner, MD. ADNI is a longitudinal multi-center study designed to develop clinical, imaging, genetic, and biochemical biomarkers for detection and prognosis of AD. Appropriate Institutional Review Board approvals occurred at each ADNI site and informed consent in accordance with the Declaration of Helsinki was obtained from each participant or authorized representative. All ADNI participants were between 55 and 90 years old, had at least 6 years of education, and were free of any significant neurological disease or systemic illness. We included only participants with baseline and follow-up 3.0-Tesla 2D FLAIR images obtained at least 2 years apart from the ADNI-GO and ADNI 2 studies in the present analyses ($n = 368$).

2.2 | Clinical Dementia Rating (CDR)

Experienced clinicians conducted semi-structured interviews with each participant and a knowledgeable collateral source. The Clinical Dementia Rating (CDR) scale was used to evaluate a participant's degree of impairment. A score of CDR 0 indicates that the individual is cognitively normal, CDR 0.5 corresponds to very mild dementia,

and CDR ≥ 1 specifies mild-to-moderate dementia. Participants with a score of CDR > 0 had a clinical diagnosis of dementia due to AD. Individuals were considered symptomatic if they had a CDR score > 0.

2.3 | *APOE* Status

APOE genotyping for all participants was extracted from the ADNI database as previously described.[18] For *APOE* analyses, individuals were grouped according to the number of ε4 alleles (none, one, or two).

2.4 | Positron emission tomography (PET) processing

Florbetapir positron emission tomography (PET) scan date was matched to the closest baseline magnetic resonance (MR) imaging date for each participant, and the summary values were extracted from the ADNI database derived from a post-reconstruction processed format. Processing steps included co-registration and averaging of the individual PET frames and orientation to the anterior commissure-posterior commissure-PC line. Full details of the processing steps can be found online (https://adni.loni.usc.edu/methods/pet-analysis-method/pet-analysis/#pet-pre-processing-container). For this study, we used the global cortical standardized uptake value ratios (SUVRs) with the cerebellum serving as a reference region (https://adni.loni.usc.edu/methods/pet-analysis). Global amyloid-positivity was defined and downloaded from the ADNI database using the cutoff value SUVR > 1.[19,20]

2.5 | White matter hyperintensity regional volume

All detailed acquisition steps for the FLAIR and MR images are available at the ADNI website (https://adni.loni.usc.edu/methods/). FLAIR images were brain extracted, bias field corrected, and were subsequently normalized using a modified Z-score transformation with 2*SD for intensity standardization across all participant images. Further preprocessing details and methodologies regarding the automated WMH segmentation pipeline have been previously described.[17] Following WMH segmentation, each individual's T1-weighted map was warped to the corresponding FLAIR timepoint. A mid-space was then made with halfway warps created from a variation of siena_flirt in the Oxford Centre for Functional Magnetic Resonance Imaging of the Brain (FMRIB)'s Software Library (FSL) using the linear warp matrix and inverse warp matrix between the two FLAIR timepoints. After aligning the T1-weighted timepoints together in a halfway space we averaged the two T1-weighted timepoints together and then proceeded to create the registration matrix to the International Consortium of Brain Mapping (ICBM) template space. This was performed with both linear and nonlinear registration tools from FSL.[21,22] The corresponding halfway space and template warp matrices generated from the average T1-weighted image in halfway space were then applied to the corresponding FLAIR and WMH segmentation images. We derived region-based longitudinal WMH volume change for each of the five etiology-specific WMH spatial patterns by subtracting WMH burden for timepoint 1 (TP1) from timepoint 2 (TP2) within regions demarcated by each WMH spatial pattern (Supplemental F1). This provided a metric of WMH volume change, and this term will be used throughout the paper to refer to the output for the standard longitudinal WMH methodology (evaluation of WMH volume vs shape change in predicting AD for further details). WMH volumes were not normally distributed and were log transformed for both TP1 and TP2.

RESEARCH IN CONTEXT

1. **Systematic review**: The following key words were used to determine the bulk of the background literature: "WMH", "longitudinal", "AD", "aging", "ADNI", "amyloid", and "tau". The lead author JS perused all literature prior to citation.
2. **Interpretation**: We describe a new technique for evaluating longitudinal WMH data and present new findings pertaining to WMH growth in an AD cohort.
3. **Future directions**: Replication studies with the shape analyses proposed in this study are needed for validation. Additionally, further research with longitudinal biomarkers for amyloid and tau would better address the underlying correlates of AD-specific WMH shape changes over time.

2.6 | White matter hyperintensity (WMH) regional expansion

Figure 1 is a visual schematic that demonstrates the overall concept of quantifying WMH expansion with regard to distance. As the white matter lesion expands over time, regardless of uniformity, the distance between the ROI and lesion boundaries would shrink representing WMH expansion. WLMA was conducted on each of the etiology-specific WMH spatial patterns in template space (Montreal Neurological Institute). First, the pattern boundary is created from the voxels that reside on the outer edge of each WMH spatial pattern (Supplemental F1). Distance maps were then generated for each of the WMH spatial patterns across all participants and for both time points. The intensity values for the pattern boundary voxels were defined as the Euclidean distance from each boundary voxel to the first lesion voxel within the confines of the corresponding pattern. This operation was performed using distancemap as part of FMRIB's Integrated Registration and Segmentation Tool (FIRST), a package for gray matter shape analysis.[23] It should be emphasized that throughout the paper we will only refer to WMH expansion/reduction as the output from the

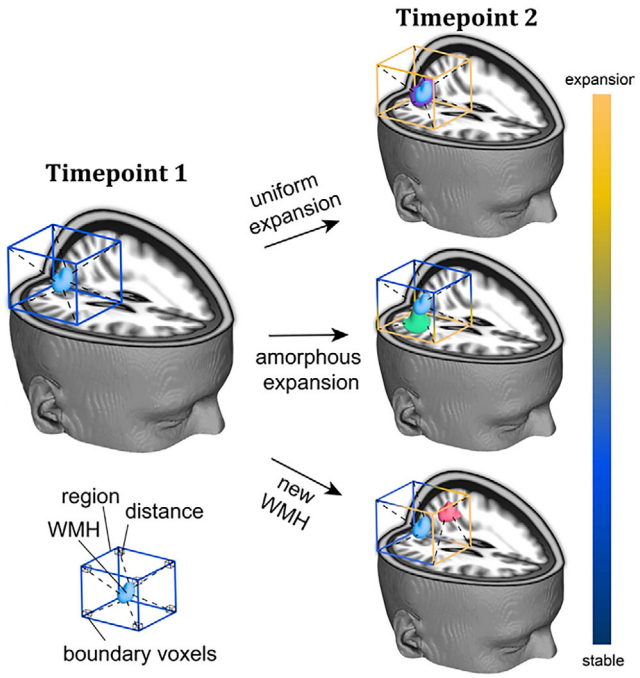

FIGURE 1 Example schematic of the white matter hyperintensity (WMH) longitudinal morphometric analysis (WLMA) technique for capturing WMH expansion. The blue translucent box (region) represents a WMH cluster. As the WMH (teal structure) expands from timepoint 1 to timepoint 2, that change is reflected along the box's outer edge as a change in distance visually depicted as the transformation from blue to yellow.

WLMA methodology (evaluation of WMH volume vs shape change in predicting AD for further details).

Distance difference (DD) maps were created by subtracting the TP2 from TP1 WMH maps where greater positivity represented increased WMH expansion (Figure 2C). Average DD maps were constructed at the voxel level for each of the five WMH spatial patterns and combined qualitatively to observe localized patterns of expansion or reduction across all participants. This process allows the distance measurements to be spatially fixed by performing the analyses on the boundaries with subject specific intensity values rather than spatially distinct WMH clusters.

2.7 | WMH association with AD process

Participants were classified based on their baseline status as either cognitively normal controls (CN), principal component (PC), or AD for a voxel-wise analysis of variance (ANOVA) across each WMH spatial pattern. CN individuals were defined as CDR = 0 with low levels of amyloid-PET (amyloid SUVR < 1.1). PC individuals were defined as CDR = 0 with elevated PET amyloid (amyloid SUVR > 1.1). AD individuals were defined as CDR > 0 with amyloid SUVR > 1.1.

WMH volume change for each WMH pattern was compared across the three groups with an omnibus ANOVA. Bonferroni correction was used to address multiple comparisons yielding a $P < 0.01$ as our threshold for significance. Subsequently, *t*-tests were performed for any pattern that survived our statistical threshold for the ANOVA.

The WLMA-based DD maps (WMH expansion) were evaluated across groups at the voxel-level pattern boundary. The voxel-wise ANOVA was performed to assess WMH expansion across the three groups. This analysis was conducted with Randomise,[24,25] the statistical toolbox in FSL. A statistical threshold of $P < 0.05$ corrected for multiple comparisons was performed using 5000 Monte Carlo permutations and threshold-free clustering. For significant patterns, voxel-wise *t*-tests were performed to determine the group or groups driving the effect using the same statistical parameters as described in the ANOVA.

2.8 | DD regional map association with amyloid and *APOE*

Voxel-wise correlations were performed between the WMH spatial patterns' DD maps and baseline PET amyloid summary values. *APOE* status was evaluated with voxel-wise ANOVA for each WMH pattern comparing WMH expansion and *APOE* ε4 allele frequency. Both the correlation and ANOVA were performed on the DD maps for all patterns analyzed with Randomise. All comparisons used a statistical threshold of $P < 0.05$ corrected for multiple comparisons with the false discovery rate and performed using 5000 Monte Carlo permutations and threshold-free clustering.

2.9 | Evaluation of WMH volume versus shape change in predicting AD

We hypothesized that voxel-wise WLMA, which incorporates etiology-specific WMH spatial pattern information, is more sensitive and specific for AD-related WMH changes. We implemented two different machine-learning (ML) classifier algorithms using Python library *Scikit-learn*. We applied support vector machine (SVM) and random forest (RF) classifiers to test whether WLMA is a more selective feature compared to longitudinal changes in total and regional WMH volumes for predicting AD versus CN. We made comparisons across different ML algorithms to demonstrate if WLMA was more robust for predicting AD. The ML experiments were performed on only the AD and control study cohort ($n = 230$), and consisted of two steps: feature selection, followed by the actual classification. For feature selection, we considered a total of 28,872 voxels with longitudinal WMH morphometric changes as potential features for WLMA, identified 274 principal components using principal component analysis, then utilized Kruskal-Wallis feature selection with a threshold of $P < 0.10$ to select 22 principal components as discriminative input features of WLMA. In a separate region-based analysis, we performed similar feature selection as above restricted to voxels within the boundaries of each of the five previously-defined WMH spatial patterns resulting in 21 to 30 principal components representing longitudinal WMH morphometric changes for each WMH spatial pattern. In contrast, six input features

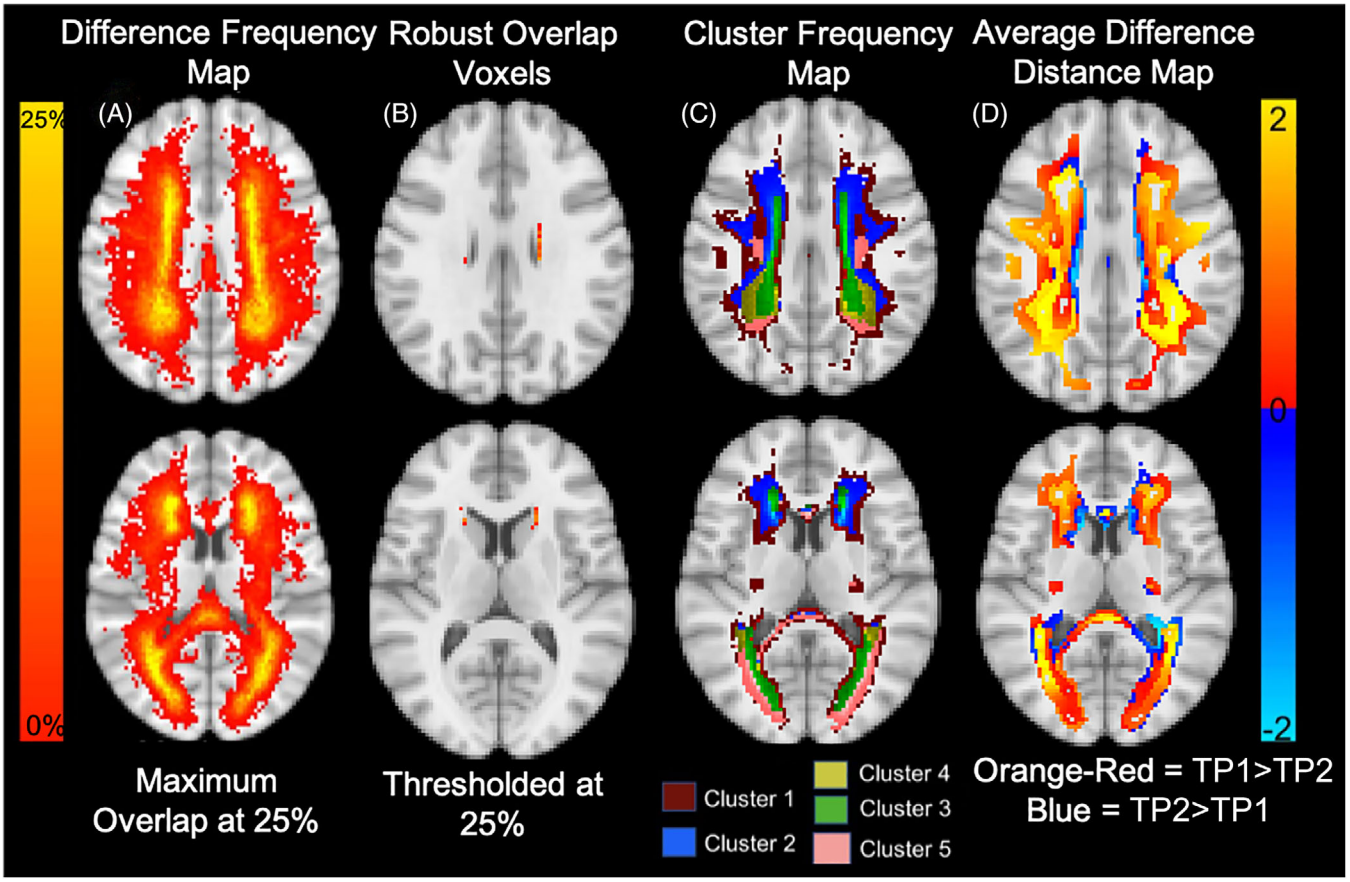

FIGURE 2 (A) Shows the difference frequency map, created by subtracting the timepoint 1 (TP1) from timepoint 2 (TP2) white matter hyperintensity (WMH) maps, with a range of WMH overlap from 0% to maximum of 25%. Increased intensity represents greater overlap. (B) Isolation of the robust maximum overlap for WMH volume. (C) WMH distribution across all five clusters. (D) Average difference distance map. Units are in mm.

were selected as representative of longitudinal WMH volume changes (global and regional WMH based on the etiology-specific WMH spatial patterns). We utilized a 70%–30% train–test split with 160 individuals randomly selected as the training and validation dataset, whereas 68 individuals formed the test dataset that was later used to test the ability of the final ML models to predict AD. Model training, validation, and testing were performed using repeated fivefold cross validation with 10 iterations. Hyperparameter optimization was performed within validation sets for SVM (kernel type, and regularization strength), and for RF (the number of trees, the depth of each tree, and the number of features selected for determining tree split), using *GridSearchCV* to obtain the combination of hyperparameters that maximizes model performance. Model performance was evaluated on the test sets by measuring performance indices of accuracy (percent correctly classified), recall (sensitivity), precision (positive predictive value), and F1-Score (harmonic mean of precision and recall) for SVM- and RF-based models using WLMA and volumetric-based features separately. McNemar's test was applied to explore for significant differences in prediction accuracies between different feature types (WLMA vs volumetry-based) and different ML classifier algorithms.

3 | RESULTS

3.1 | Demographics

A total of 368 individuals with a baseline assessment plus at least one follow-up assessment >2 years later were included in our study. Of these, 98 individuals were excluded from analyses for exhibiting non-AD pathology ($n = 93$), poor registration ($n = 4$), and poor scan quality ($n = 1$). This yielded a total of 270 individuals that were included into the following analyses ($n = 270$: 98 CN, 42 PC, and 130 AD) (Supplemental F2). Further details are provided in Table 1. The average time period between TP1 and TP2 was 3 years with a standard deviation of 1.02 years. For this analysis cohort, no group differences across all three groups were observed for age, education, or race. There were differences in sex distribution by diagnosis group: more females were CN, whereas the PC group had a greater proportion of males. The ML analysis was only performed on the AD and CN groups resulting in 228 individuals. Baseline demographic and clinical variables including *APOE* ε4 genotype and years of education were extracted for our study cohort.

TABLE 1 Demographics table for each of the disease stages and the non-AD group.

	Control	Preclinical	AD	*P*-value
N	98	42	130	NA
Age (years)	71 (6.0)	74 (6.05)	73 (6.83)	0.07
Gender (M/F)	46/52	23/16	73/58	0.014
Education (years)	17 (2.43)	16 (2.7)	16 (2.65)	0.17
Race				
Amyloid	1.02 (0.05)	1.32 (0.19)	1.36 (0.17)	<0.001
Hypertension	4.1 (2.63)	4.2 (3.36)	4.2 (3.67)	0.84
*APOE e*4 status (0,1,2)	76/20/2	23/17/2	47/62/21	<0.001
Time gap (years)	3 (1.07)	2.9 (1.14)	3 (1.05)	0.88

Note: Statistics are reported as mean (SD). Hypertension was based on binary clinical classification. The *P*-values represent the findings from an ANOVA between each disease stage not including the non-AD group.
Abbreviation: AD, Alzheimer's disease.

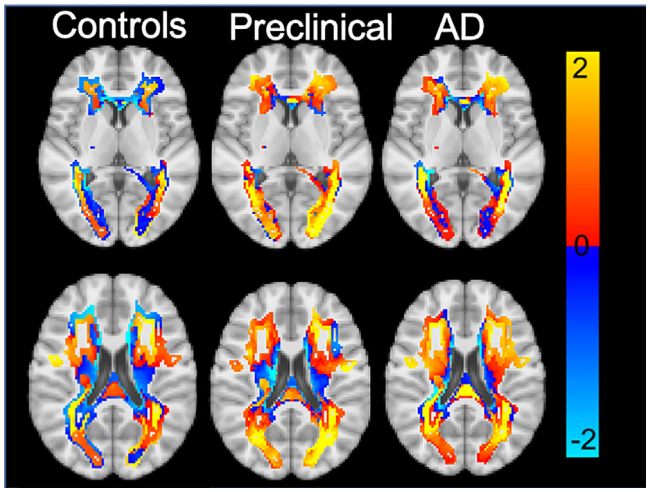

FIGURE 3 Average difference distance maps across all clusters for each disease stage. Units are in mm. AD, Alzheimer's disease.

3.2 | Changes in regional WMH volume versus expansion

At the group level, traditional approaches at quantifying WMH data rely on the frequency overlap of lesions and can be insensitive to spatially specific WMH changes. This can be challenging as WMH are often spatially distinct and small deviations in location can result in no overlap despite similar spatial localization. This issue for determining WMH spatial patterns is compounded for longitudinal data as region-based WMH analyses have greater reliance on lesion overlap across time (Figure 2A,B). Figure 2A is a frequency overlap map based on WMH volume change. The intensity maximum threshold was observed at 25% across the entire cohort (Figure 2B) with very little overlap in WMH volume change. Although individually, WMH volume change is diffusely present across the entire brain (Figure 2A), analyses restricted by lesion frequency are more limited in group comparisons (Figure 2B).

WMH expansion was observed across all participants from TP1 to TP2 (Supplemental F3). Unlike WMH volume, WLMA does not rely on lesion voxel overlap to evaluate WMH spatial information. Although brain structures are aligned based on the registration matrices to template space the WMH clusters among individuals can be innately distinct at the voxel level. Spatial information is preserved without sacrificing statistical power because WLMA quantifies shifts in WMH boundaries at the individual level that we refer to as WMH expansion. Analyzing the data in this manner incorporates the changes in individual level WMH morphometrics across timepoints allowing for evaluation at the voxel level (Figure 2C,D). Figure 2C is the same WMH frequency overlap map as seen in Figure 2A but organized by the five WMH patterns. The main point is the distinction between Figure 2B and Figure 2D which highlights the benefit of evaluating WMH expansion as opposed to WMH volume. When considering differences in WMH volume 86% of individuals are not represented in Figure 2B whereas all participants contributed to the statistical analyses of WMH expansion.

3.3 | WLMA with AD process

The average DD maps for each group (AD, PC, CN) are represented across all WMH spatial patterns in Figure 3. The quantitative ANOVA revealed that only the periventricular WMH patterns had significantly different rates of change in WMH expansion across all three groups (CN, PC, AD). Paired *t*-tests revealed this difference was driven by greater expansion of WMH for the preclinical compared to the CN group but not the AD group (Supplemental F4). The AD group was also not significantly different from preclinical group for this WMH pattern.

3.4 | DD regional map association with amyloid and *APOE*

Amyloid accumulation associated with WMH expansion in the posterior WMH pattern (Figure 4) and in the deep frontal WMH pattern across all subjects. Reanalyzing the voxel-wise correlations for the posterior and deep frontal WMH patterns within the groups individually revealed a significant association with amyloid in the deep frontal but only for the AD group (Figure 4). There was no difference observed between groups for individuals with a single *APOE* ε4 allele but 75% of the individuals with two ε4 alleles were designated as AD. The ANOVA for *APOE* status across the genetic profile revealed no significant associations with any WMH spatial pattern.

3.5 | WMH morphometric change is more predictive of AD

We compared the selectivity of WLMA and volumetric WMH change as features for different ML classifiers in predicting AD. SVM- and RF-based classifiers using WLMA features were able to more effectively and robustly identify individuals with AD compared to volumetric

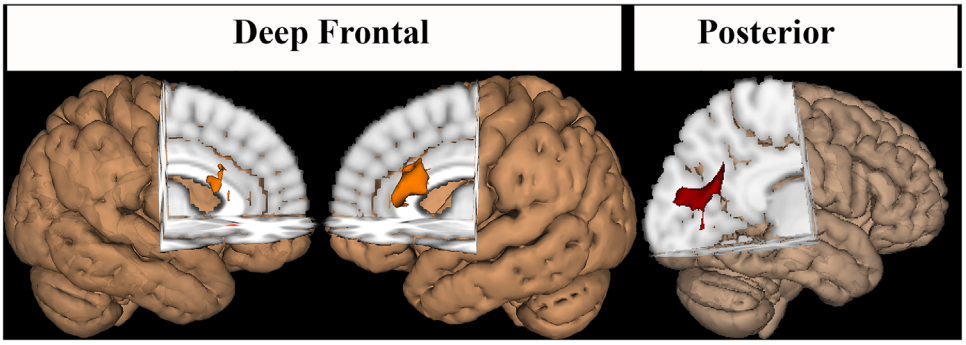

FIGURE 4 The images show the 3D rendering of where significant associations between amyloid and white matter hyperintensities (WMH) expansion were observed across all three disease stages. The deep frontal regions were driven by the dementia group that revealed a significant association within the group. The posterior region relationship between WMH expansion and amyloid was only observed across the entire group.

TABLE 2 Machine learning output comparing the prediction capabilities of WLMA and volumetrics with two machine learning methods.

	WLMA		Volumetrics	
ML Model	SVM	RF	SVM	RF
Accuracy	0.70	0.67	0.55	0.59
Sensitivity for AD (Recall)	0.67	0.74	0.37	0.70
Precision for AD	0.81	0.73	0.80	0.67
F1 score (AD)	0.73	0.74	0.51	0.68

Abbreviations: AD, Alzheimer's disease; ML, machine learning; SVM, support vector machine; RF, random forest; WLMA, white matter hyperintensity longitudinal morphometric analysis.

WMH changes across all classification performance metrics (Table 2). The McNemar's test confirmed that WMH expansion quantified with WLMA classified AD individuals with significantly greater accuracy than WMH volume (SVM, $P = 0.02$; RF, $P = 0.04$). No statistical difference was observed in prediction accuracy between ML models (WLMA: SVM vs RF, $P = 0.15$; Volume: SVM: SVM vs RF, $P = 0.68$). The confusion matrices evaluating the performance of both classifiers using WLMA and volumetric features are shown in Supplemental F5. On average, SVM and RF models using WLMA features correctly classified 70.0% and 67.0% of AD individuals, with sensitivity of 0.67 and 0.74, and specificity of 0.81 and 0.73, respectively. For the region-based WMH analysis, WMH morphometric change for both periventricular and parietal WMH patterns had the highest sensitivity for predicting AD for both SVM (0.88 and 0.81) and RF (0.88 and 0.84) classification models.

4 | DISCUSSION

In this study, we assessed a novel application of lesion shape analysis to evaluate WMH expansion in AD over an average 3-year period. Compared to standard WMH volume metrics, WLMA repeatedly outperformed classical approaches for identifying unique WMH changes over time in our PC group and in distinguishing controls from AD with ML-based prediction models. The preclinical (CDR = 0) individuals demonstrated WMH expansion in distinct posterior periventricular WM regions but increasing amyloid burden in the AD individuals was associated with greater WMH expansion in frontal regions.

The literature is divided on the role of WMH in AD and some have postulated that this WMH initialization process is entirely independent but may have additive effects on the process to early symptomatic stages in AD.[26] Postmortem work has found that the periventricular posterior WM region contains underlying, gliosis, and axonal loss specifically in AD individuals.[27] Conversely, WMH of non-presumed AD origin are predominantly more prevalent in frontal areas implicating spatial location as disease specific.[17,28] Evidence to support separate mechanisms is based on a lack of evidence supporting a longitudinal link with between WMH and AD biomarkers.[29] This minimizes the role of WMH development in AD, despite strong associations with cognition and neurodegeneration.[30,31] This infers that WMH changes associate with amyloid accumulation in AD pathology but can be overlooked with methods that fail to incorporate the spatial topography.

Increased dysfunction and damage in the brain's blood vessels associates with increased Aβ formation.[32] The resultant damage to cerebral vasculature can potentially promote formation of diffuse plaques and phosphorylated tangles.[33–35] This feedforward process may explain the associations between amyloid and WMH expansion that were observed within the deep frontal and posterior WM across the entire group. However, the deep frontal association was uniquely associated with the AD group. Individuals with AD have demonstrated reduced vascular reactivity primarily in the rostral frontal cortex compared to controls independent of cardiovascular factors.[36] Similarly, pathological findings reveal frontal WMH associates with both small vessel disease and disease specific AD neurodegenerative mechanisms.[37] Our data suggest that AD individuals with greater amyloid accumulation at baseline associate with faster WMH expansion of frontal WMH within individuals with AD.

Most of the prior work involving WMH in AD only evaluated WMH as a global score, whereas regional WMH measurements may allow for more accurate interpretation.[12,15] We argue that analyzing the data as a global score, or via similar strategies like voxel-based lesion

symptom mapping, often rely on voxel-based overlap and are incapable of producing significant findings longitudinally across groups.[38] Additionally, the spatial information obtained by the aforementioned techniques cannot be applied at the voxel level effectively. However, WLMA spatially fixes the data within a given region, thereby allowing greater spatial specificity for detecting subtle changes in WMH expansion (Figure 2). This point was clearly emphasized in Figure 2, which showed very limited change in lesion overlap at 25% even though WMH expansion was diffusely prominent. WLMA allowed for more sensitive localized findings when analyzing disease stages with healthy aging or increased disease severity by identifying spatially specific changes at the voxel level.

Our study has several limitations. WLMA is not a lesion segmentation technique and we did not assess how the segmentation technique can influence the outcome of WLMA. However, the segmentation technique utilized has been shown to be reliable with manual segmentations and employs deep learning to differentiate lesions from non-lesions voxel-by-voxel.[17] The WMH patterns used to define our longitudinal region-based WMH analysis were determined from a larger cross-sectional cohort but WLMA is not restricted to these regions. Although no longitudinal information was used in the pattern calculations for deriving the WMH regions, all baseline images were involved in the original study albeit as a subset. This study focused only on global baseline levels of amyloid but longitudinal PET studies that assess regional changes would improve our understanding of WMH expansion. Although the findings from this study suggest a mechanistic link between spatially specific WMH expansion and AD, further studies that incorporate biomarkers related to other non-AD sources of variance are needed to bolster this claim. Replication of this work in another large longitudinal cohort with more detailed stroke history is necessary to validate these findings. For this study we utilized the ADNI cohort due to its large cohort size of AD-focused longitudinal data. However, the ADNI cohort is limited due to the acquisition of 2D FLAIR sequences as opposed to 3D sequences that are recently growing in popularity. Therefore, future longitudinal studies within large cohorts using 3D sequences are warranted. The focus of this study was to determine whether we could detect subtle changes in WMH expansion, and we therefore did not evaluate other stages that make up traditional ATN models to fully understand WMH's role in AD process. Acquiring longitudinal data for each stage of the ATN hypothesis in conjunction with longitudinal FLAIR would greatly improve the interpretations of the findings presented here. Lastly, this is the first application of this technique and external validation would improve its validity to the scientific community.

5 | CONCLUSION

In conclusion, we introduced a novel approach to evaluating regional WMH expansion. We demonstrated that WLMA provides similar information as WMH volume but is also more sensitive to spatial information that we demonstrate to be clinically relevant. Our analyses of individuals with AD yielded distinct localized regions of WMH expansion for cognitively impaired AD individuals and individuals at the preclinical stage without cognitive symptoms. This strongly supports the view that WMH changes continue to evolve morphometrically throughout the disease and can precede cognitive changes. Therefore, the development of WMH may play an undervalued role in AD pathogenesis and offer alternative treatment strategies.

ACKNOWLEDGEMENTS

Data collection and sharing for this project was funded by the Alzheimer's Disease Neuroimaging Initiative (ADNI) (National Institutes of Health Grant U01 AG024904) and DOD ADNI (Department of Defense award number W81XWH-12-2-0012). ADNI is funded by the National Institute on Aging, the National Institute of Biomedical Imaging and Bioengineering, and through generous contributions from the following: AbbVie; Alzheimer's Association; Alzheimer's Drug Discovery Foundation; Araclon Biotech; BioClinica, Inc.; Biogen; Bristol-Myers Squibb Company; CereSpir, Inc.; Cogstate; Eisai Inc.; Elan Pharmaceuticals, Inc.; Eli Lilly and Company; EUROIMMUN; F. Hoffmann-La Roche Ltd and its affiliated company Genentech, Inc.; Fujirebio; GE Healthcare; IXICO Ltd.; Janssen Alzheimer Immunotherapy Research & Development, LLC.; Johnson & Johnson Pharmaceutical Research & Development LLC.; Lumosity; Lundbeck; Merck & Co., Inc.; Meso Scale Diagnostics, LLC.; NeuroRx Research; Neurotrack Technologies; Novartis Pharmaceuticals Corporation; Pfizer Inc.; Piramal Imaging; Servier; Takeda Pharmaceutical Company; and Transition Therapeutics. The Canadian Institutes of Health Research is providing funds to support ADNI clinical sites in Canada. Private sector contributions are facilitated by the Foundation for the National Institutes of Health (www.fnih.org). The grantee organization is the Northern California Institute for Research and Education, and the study is coordinated by the Alzheimer's Therapeutic Research Institute at the University of Southern California. ADNI data are disseminated by the Laboratory for Neuro Imaging at the University of Southern California. This study was supported by the National Institute on Aging (NIA) grant R01 AG053550 (Dr. Xiong), NIH-NINDS (K23 NS110927), NIA (R01AG052550, R01AG057680, R01AG067103), and the American Heart Association (19CDA34620004). Further support was provided from NIH-NIA through P01 AG026276 and R01 AG052550, the Daniel J Brennan MD Fund, and the Paula and Rodger O. Riney Fund.

CONFLICTS OF INTEREST STATEMENT

Jeremy Fuller Strain: None. Chia-Ling Phuah: None. Babatunde Adeyemo: None. Kathleen Cheng: None. Kyle B. Womack: None. John McCarthy: None. Manu Goyal: None. Yasheng Chen: None. Aristeidis Sotiras: Personal compensation for serving as a grant reviewer for BrightFocus Foundation. Holds equity in TheraPanacea. Hongyu An: None. Chengjie Xiong: None. Andrea Scharf: None. Catherine Newsome-Stewart: None. John Carl Morris: He is currently participating in clinical trials of antidementia drugs developed by Eli Lilly and Company, Biogen, and Janssen. Dr. Morris serves as a consultant for Lilly USA. Research support from Eli Lilly/Avid Radiopharmaceuticals. Tammie Lee Smith Benzinger: Involved in a clinical trial sponsored by Avid. Jin-Moo Lee: None. Beau M. Ances: Involved in a clinical trial sponsored by Avid. Author disclosures are available in the supporting information.

CONSENT STATEMENT

The authors complied with the guidelines of the International Committee of Medical Journal Editors and study approval was obtained by the Human Subjects Institutional Review Board (IRB) of Washington University in St. Louis and other collaborating sites. There are no financial conflicts of interest. Appropriate Institutional Review Boards approval occurred at each ADNI site and informed consent in accordance with the Declaration of Helsinki was obtained from each participant or authorized representative.

REFERENCES

1. Jack CR, Bennett DA, Blennow K, et al. NIA-AA Research Framework: toward a biological definition of Alzheimer's disease. *Alzheimers Dement*. 2018;14:535-562.
2. Vemuri P, Lesnick TG, Przybelski SA, et al. Age, vascular health, and alzheimer disease biomarkers in an elderly sample. *Ann Neurol*. 2017;82:706-718.
3. Prins ND, Scheltens P. White matter hyperintensities, cognitive impairment and dementia: an update. *Nat Rev Neurol*. 2015;11:157-165.
4. Kim HW, Hong J, Jeon JC. Cerebral small vessel disease and Alzheimer's disease: a review. *Front Neurol*. 2020:11–927. doi:10.3389/fneur.2020.00927
5. Wong FCC, Saffari SE, Yatawara C, et al. Influence of white matter hyperintensities on baseline and longitudinal amyloid-B in cognitively normal individuals. *J Alzheimers Dis*. 2021;84:91-101.
6. Walsh P, Sudre CH, Fiford CM, et al. CSF amyloid is a consistent predictor of white matter hyperintensities across the disease course from aging to Alzheimer's disease. *Neurobiol Aging*. 2020;91:5-14.
7. Luo X, Jiarken Y, Yu X, et al. Associations between APOE genotype and cerebral small-vessel disease: a longitudinal study. *Oncotarget*. 2017;8:44477-44489.
8. Zhao C, Strobino K, Moon YP, et al. APOE e4 modifies the relationship between infectious burden and poor cognition. *Neurology*. 2020. doi:10.1212/NXG.0000000000000462
9. Youjin J, Raymond V, Sanneke R, et al. White matter hyperintensities and apolipoprotein e affect the association between mean arterial pressure and objective and subjective cognitive functioning in older adults. *J Alzheimers Dis*. 2021;84:1337-1350.
10. Wang Y, Chen W, Cai W, et al. Associations of white matter hyperintensities with cognitive decline: a longitudinal study. *J Alz Dis*. 2020. doi:10.3233/JAD-191005
11. Carmichael O,chwarz C, Drucker D, et al. Longitudinal changes in white matter disease and cognition in the first year of the Alzheimer disease neuroimaging initiative. *Arch Neurol*. 2010;67:1370-1378.
12. Rizvi B, Lao PJ, Chesebro AG, et al. Association of regional white matter hyperintensities with longitudinal Alzheimer-like pattern of neurodegeneration in older adults. *JAMA Neurol*. 2021;4:10-32125166.
13. Lampe L, Kharabian-Masouleh S, Kynast J, et al. Lesion Location matters: the relationships between white matter hyperintensities on cognition in the healthy elderly. *J Cereb Blood Flow Metab J Cerebr Blood F Met*. 2019. doi:10.1177/0271678İ17740501
14. Biesbroek JM, Lam BYK, Zhao L, et al. High white matter hyperintensity burden in strategic white matter tracts relates to worse global cognitive performance in community-dwelling individuals. *J Neurol Sci*. 2020;414:116835.
15. Brickman AM, Provenzano FA, Muraskin J, Manly JJ, Blum S, et al. Regional white matter hyperintensity volume, not hippocampal atrophy, predicts incident Alzheimer disease in the community. *Arch Neurol*. 2012;69:1621-1627.
16. Habes M, Sotira A, Erus G, et al. White matter lesions spatial heterogeneity, links to risk factors, cognition, genetics and atrophy. *Neurology*. 2018;91. doi:10.1212/WNL.0000000000006116
17. Phuah C, Chen Y, Strain JF, et al. Association of data-driven white matter hyperintensity spatial signatures with distinct cerebral small vessel disease etiologies. *Neurology*. 2022;10. WNL.0000000000201186
18. Saykin AJ, Shen L, Foroud TM, Potkin SG, Swaminathan S, et al. Alzheimer's Disease Neuroimaging Initiative biomarkers as quantitative phenotypes: genetics core aims, progress, and plans. *Alzheimer Dementia*. 2010;6:265-273.
19. Joshi A, Pontecorvo M, Breault C, et al. Use of florbetapir-PET to assess progression of amyloid burden over time. *J Nuclear Medicine*. 2012;53:89.
20. Landau SM, Jagust WJ, Florbetapir processing methods. 2015, https://adni.bitbucket.io/reference/docs/UCBERKELEYAV45/ADNI_AV45_Methods_JagustLab_06.25.15.pdf
21. Jenkinson M, Smith SM. A global optimization method for robust affine registration of brain images. *Med Image Anal*. 2001;5:143-156.
22. Jenkinson M, Bannister PR, Brady JM, Smith SM. Improved optimization for the robust and accurate linear registration and motion correction of brain images. *Neuroimage*. 2002;17:825-841.
23. Patenaude B, Smith SM, Kennedy D, Jenkinson M. A Bayesian model of shape and appearance for subcortical brain. *Neuroimage*. 2011;56:907-922.
24. Winkler AM, Ridgway GR, Webster MA, Smith SM, Nichols TE. Permutation inference for the general linear model. *Neuroimage*. 2014;92:381-397.
25. Anderson MJ, Robinson J. Permutation tests for linear models. *Aust New Zeal J Stat Stat*. 2001;43:75-88.
26. Soldan A, Pettigrew C, Zhu Y, et al. White matter hyperintensities and CSF Alzheimer disease biomarkers in preclinical Alzheimer disease. *Neurology*. 2019;94. WNL.000000000008864.
27. Alber J, Alladi S, Bae HJ, et al. White matter hyperintensities in vascular contributions to cognitive impairments and dementia (VCID): knowledge gaps and opportunities. Alzheimer's. *Dement Transl Res Clin Interv*. 2019;5:107-117.
28. Palhaugen L, Sudre CH, Tecelao S, et al. Brain amyloid and vascular risk are related to distinct white matter hyperintensity patterns. *J Cereb Blood Flow Metab*. 2021;41:1162-1174.
29. Dodge HH, Zhu J, Harvey D, et al. Biomarker progressions explain higher variability in specific cognitive decline than baseline values in Alzheimer disease. *Alzheimers Dement*. 2014:690-703.
30. Mielke MM, Frank RD, Dage JL, et al. Comparison of plasma phosphorylated tau species with amyloid and tau positron emission tomography, neurodegeneration, vascular pathology, and cognitive outcomes. *JAMA Neurol*. 2021;78:1108-1117.
31. Schwarz CG, Knopman DS, Vijay RK, et al. Longitudinally increasing elevated asymmetric flortaucipir binding in a cognitively unimpaired amyloid-negative older individual. *J Alzheimers Dis*. 2022;85:59-64.
32. Karran E, De Strooper B. The amyloid cascade hypothesis: are we poised for success or failure? *J Neurochem*. 2016;139:237-252.
33. Cox SR, Lyall DM, Ritchi SJ, et al. Associations between vascular risk factors and brain MRI indices in UK Biobank. *Eur Heart J*. 2019;28:2290-2300.
34. De la T, Jack C. Cerebral hemodynamics and vascular risk factors: setting the stage for Alzheimer's disease. *J Alzheimer Dise*. 2012;32(3):553-567.
35. Sweeney MD, Kisler K, Montagne A, Toga AM, Zlokovic BV. The role of brain vasculature in neurodegenerative disorders. *Nat Neuroscie*. 2018;21:1318-1331.
36. Yezhuvath US, Uh J, Cheng Y, et al. Forebrain-dominant deficit in cerebrovascular reactivity in Alzheimer's disease. *Neurobiol Aging*. 2012;33:75-82.
37. McAleese KE, Miah M, Graham S, et al. Frontal white matter lesions in Alzheimer's disease are associated with both small vessel disease and AD-associated cortical pathology. *Acta Neuropathol*. 2021;142:937-950.

38. Kimberg DY, Coslett HB, Schwartz MF. Power in voxel-based lesion-symptom mapping. *J Cogn Neurosci*. 2007;19:1067-1080.

SUPPORTING INFORMATION

Additional supporting information can be found online in the Supporting Information section at the end of this article.

How to cite this article: Strain JF, Phuah C-L, Adeyemo B, et al. White matter hyperintensity longitudinal morphometric analysis in association with Alzheimer disease. *Alzheimer's Dement*. 2023;19:4488–4497.
https://doi.org/10.1002/alz.13377